

CrystEngComm

Accepted Manuscript



This is an *Accepted Manuscript*, which has been through the Royal Society of Chemistry peer review process and has been accepted for publication.

Accepted Manuscripts are published online shortly after acceptance, before technical editing, formatting and proof reading. Using this free service, authors can make their results available to the community, in citable form, before we publish the edited article. We will replace this *Accepted Manuscript* with the edited and formatted *Advance Article* as soon as it is available.

You can find more information about *Accepted Manuscripts* in the [Information for Authors](#).

Please note that technical editing may introduce minor changes to the text and/or graphics, which may alter content. The journal's standard [Terms & Conditions](#) and the [Ethical guidelines](#) still apply. In no event shall the Royal Society of Chemistry be held responsible for any errors or omissions in this *Accepted Manuscript* or any consequences arising from the use of any information it contains.

Cite this: DOI: 10.1039/c0xx00000x

www.rsc.org/xxxxxx

ARTICLE TYPE

Structural framework of biologically active coumarin derivatives. Crystal structures and Hirshfeld surface analysis

Magdalena Malecka,^{*a} Elzbieta Budzisz^b

Received (in XXX, XXX) Xth XXXXXXXXXX 20XX, Accepted Xth XXXXXXXXXX 20XX

DOI: 10.1039/b000000x

A series of three biologically active coumarin derivatives have been synthesised and their crystal structures have been determined from single X-ray analysis. The interactions between molecules were characterised by different synthons and via Hirshfeld surface analysis. The characteristic features of all structures are 2D sheets of molecules formed by C-H...O hydrogen bonds, which are enhanced by π ... π interactions or C-H...O interactions. Additionally, the lipophilicity parameter (logP) which describes the compound's ability to go through membranes was compared with respect to different intermolecular interactions. It was found that higher lipophilicity is associated with a larger contribution of C-H... π interactions in the crystal packing.

Introduction

Noncovalent molecular interactions such as hydrogen bonds and aromatic π ... π stacking interactions form the basis of the design of the supramolecular arrangement in organic crystals.¹ The functional substituents such as amino, hydroxyl, carbonyl groups etc. play an important role in the spatial arrangement of the neighbouring molecules, leading to repeated hydrogen bond patterns or supramolecular assemblies.² Therefore, it is useful to study structural features as well as the interplay of noncovalent interactions when building possible supramolecular synthons.

In recent years, the discovery that coumarins have weak estrogenic activity has resulted in the use of such derivatives as therapeutic agents to prevent the emergence of menopause related diseases, such as osteoporosis, an increased risk of cardiovascular event/ disease and cognitive deficiencies.³ Coumarin and its derivatives are an interesting group of compounds with spasmolytic, antiarrhythmic, cardiotonic, photodynamic⁴ and antitumor properties.⁵ These compounds are widely distributed throughout nature and a lot of them possess useful and diverse biological activities.⁶ Coumarins have been found to have numerous therapeutic applications including phototherapy, as central nervous system stimulants and as selective estrogen receptor modulators.⁷

The coumarins presented here (Fig. 1), originate from the group of derivatives, for which the biological activity has been proven.⁸ In this paper we present the crystal structure of three coumarins with respect to intermolecular interactions in the crystal lattice, which undoubtedly play an important role in the arrangement of the molecules in the crystal packing.⁹ We investigate crystal packing via the Hirshfeld surface¹⁰ and the breakdown of corresponding fingerprint plots revealing significant intermolecular interaction differences between compounds.

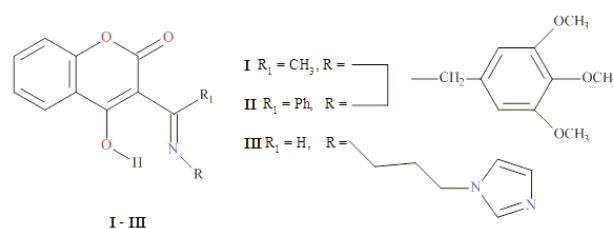


Fig. 1 Scheme of investigated compounds

Furthermore, systematic structural studies of biologically active compounds enables the relations between biological activity and unique structural features to be observed. This always supports a design of biologically active compounds. Among many parameters indicative of the biological activity we have focused on the lipophilicity which is responsible for transport into the cells.¹¹ The aim of this paper is to investigate how different interactions and crystal packing are related to lipophilicity.

Experimental section

General procedure for the synthesis of compounds (I), (II), (III).

A methanol solution (10mL) containing 1mmol of methyl ester of 2-methylchromone-3-carboxylic acid (for I), ethyl ester of 2-phenylchromone-3-carboxylic acid (for II) and methyl ester of chromone-3-carboxylic acid (for III) was added to 1mmol of the corresponding amine (3,4,5-trimethoxybenzylamine – for I & II and 1-(3-aminopropyl)imidazole - for III). The reagents were left for 24 hours at room temperature. Next the precipitated solid was filtered off and washed with ethyl ether and dried. The overall reaction is presented in Scheme S1.

The melting points were visually determined using Büchi540 apparatus and are uncorrected. The IR and far-IR spectra were

Cite this: DOI: 10.1039/c0xx00000x

www.rsc.org/xxxxxx

ARTICLE TYPE

Table 1 Crystallographic parameters for compounds (I), (II) and (III) at 100K

	compound (I)	compound (II)	compound (III)
Empirical formula	C ₂₁ H ₂₁ NO ₆	C ₂₆ H ₂₃ N ₁ O ₆	C ₁₆ H ₁₅ N ₃ O ₃
Molecular weight	383.39	445.47	297.31
Size (mm)	0.04 x 0.05 x 0.44	0.1 x 0.1 x 0.24	
Crystal system	monoclinic	monoclinic	monoclinic
Space group	P2 ₁	P 2 ₁ /c	P 2 ₁ /c
a[Å]	4.683(1)	11.415(1)	8.166(3)
b[Å]	13.113(1)	15.581(1)	17.642(3)
c[Å]	14.708(1)	15.059(1)	10.775(4)
β[°]	90.090(2)	126.999(1)	117.060(2)
V[Å ³]	905.1(1)	2139.1(2)	1382.3(7)
Z/ d _s [g cm ⁻³]	2/ 1.407	4	4
μ[mm ⁻¹]	0.104	0.099	0.097
λ[Å]	0.71073	0.71073	0.6000
max θ[°]	26.49	25.00	21.72
No. of measured reflections	7997	14059	54389
No. of unique reflections	3657	3760	2668
R _(int)	0.0357	0.0351	0.0307
No. of observed reflns (I>2 σ(I))	2490	2595	2528
Data/restraints/parameters	3657/1/262	3760/0/325	2668/0/203
R ₁ (obsd data)	0.0574	0.0555	0.0366
R ₁ (all data)	0.0337	0.0331	0.0355
Goodness-of-fit on F ²	0.800	0.861	1.031
largest difference peak and hole [e/Å ³]	0.167/-0.145	0.170-0.182	0.269/-0.296

^a Footnote text.

recorded on FT-IR-8400S Shimadzu in KBr pellets. The ¹H NMR spectra were recorded on a Varian Gemini 200 BB, CDCl₃, 200 MHz. The EI-MS data were determined using a Finnigan Matt 95 mass spectrometer. Satisfactory elemental analyses (within ±0.4% of the calculated values) were obtained for the new compounds in the Microanalytical Laboratory of the Department of Bioorganic Chemistry (Medical University, Lodz) using a Perkin Elmer PE 2400 CHNS analyser.

Compound (I) m.p = 193.2-197.3°C IR(KBr) [cm⁻¹]: 3443 ν (N-H), 3003 ν (C-H), 1703 ν(C=O), 1614 ν (N=C), 1597, 1576 ν(aromat.), 1512, 1468 δ(aromat.), 1134 ν(C-O-C), 1003 ν(O-C), 957 τ (C_{Ar}-H), 760, 715 γ(C_{Ar}-H, out-of-plane) 434 γ(C=O).

Elemental Analysis C₂₁H₂₁NO₆ (383.39 g/mol) Calc. C 65.79, H 5.52, N 3.65. Found. C 65.60, H 5.33, N 3.66 %. ¹H NMR (CDCl₃ δ ppm) 2.78 (3H, s, CH₃), 3.86 (s, 9H, OCH₃), 4.66 (2H, d, J = 5.9 Hz, CH₂), 6.42 (1H, d, J = 8.2 Hz, H₅ aromat), 6.96(2H, s, H_{2',6'} aromat.), 7.03 (1H, d, J = 8.2 Hz, H₈), 7.45(2H, 2x t, H₆, 20 H₇), 14.54 (1H, s, OH).

Compound (II) m.p = 150.4-151.5°C IR(KBr) [cm⁻¹]: (C-O-C), [cm⁻¹] 3067 ν (C-H), 1723 ν (C=O), 1605 ν(N=C), 1592, 1560 ν(aromat.), 1504, 1465 δ(aromat.), 1125 ν(C-O-C), 1013 ν(O-C), 942 τ(C_{Ar}-H), 764, 706 γ(C_{Ar}-H, out-of-plane), 464 γ(C=O).

Elemental Analysis C₂₆H₂₃NO₆ (445.46 g/mol) Calc. C 70.10, H 5.20, N 3.14. Found. C 70.14, H 4.91, N 3.27 %. ¹H NMR (CDCl₃ δ ppm) 3.84 (s, 9H, OCH₃), 4.65 (2H, d, J = 5.9 Hz, CH₂), 6.65 (2H, s, H_{2',6'}), 6.98 (2H, 2xt, H₆, 7), 7.24 (1H, d, J = 8.2 Hz, H₅ aromat), 7.52 (3H, m, H_{3',4',5'}), 7.71 (1H, d, J = 5.9 Hz,

8.01 (2H, d, J = 8.2 Hz, H_{2',6'}), 9.91 (1H, s, OH)

Compound (III) m.p = 164.6-165.6°C IR(KBr) [cm⁻¹]: 3139 ν(N-H), 2930 ν(C-H), 1713 ν(C=O), 1635 ν(N=C), 1595, 1562 ν(aromat.), 1464 δ(aromat.), 1128, 1102 ν(C-O-C), 1082 ν(O-C), 1028 τ(C_{Ar}-H), 753 τ(C_{Ar}-H, out-of-plane), 671 ω(N-H), 445 γ(C=O). Elemental Analysis C₁₆H₁₅N₃O₃ (297.11 g/mol) Calc. C 64.64, H 5.09, N 14.13. Found. C 64.43, H 4.19, N 14.27 %. ¹H NMR (CDCl₃ δ ppm) 2.03 (2H, t, CH₂), 3.25 (2H, 2xt, CH₂), 3.38 (2H, t, CH₂), 6.51 (1H, s, C≡H), 6.97 (1H, s, C≡H), 7.08 (2H, 2xt, H₆, 7), 7.36 (1H, d, J = 8.1 Hz, H₅ aromat), 7.54 (2H, 2xd, 40 H_{4',5'}), 7.96 (1H, d, J = 5.9 Hz, H₈), 12.71 (1H, s, OH).

Data collection, structure solution and refinement

Data for compound I and II were measured from single crystals using an Oxford Diffraction Xcalibur CCD diffractometer at T=100(2) K with monochromatic MoKα radiation (λ=0.71073 Å). Data reduction was performed using CrysAlis software.¹² Data were corrected for Lorentz and polarisation effects; absorption correction was not applied.

Diffraction data for compound III were collected at the F1 beamline of storage ring DORIS III at HASYLAB/DESY in Hamburg. The beamline is equipped with a Huber 4-circle diffractometer with MARCCD 165. The temperature was maintained at 100(1) K and the wavelength was (λ= 0.6000 Å). The integration, data reduction and scaling of diffracted intensities were performed using the XDS package version 55 2009.¹³ At this point intensities were corrected for oblique

incidence of X-rays on the detector surface.¹⁴

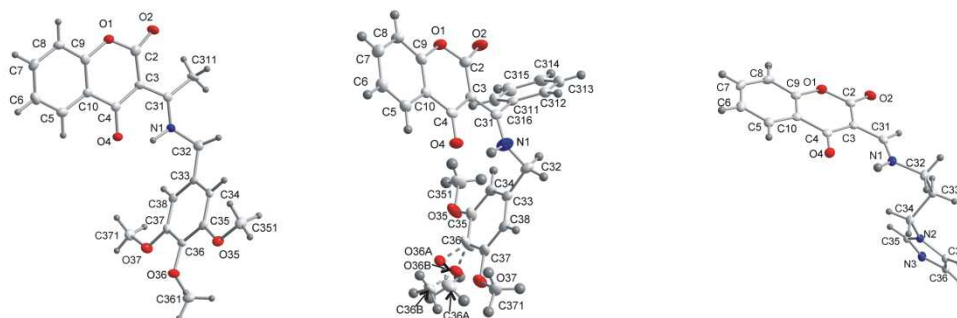


Fig. 2 An ORTEP view and atom numbering scheme of compound (I), (II) and (III) with displacement ellipsoids at the 30% probability level. Hydrogen atoms are shown as small spheres of arbitrary radii

5 All structures were solved by direct methods with SHELXS97¹⁵ and further refined on F^2 using SHELXL97.¹⁵ A full matrix least-squares refinement procedure was used. The methoxy group in compound II was disordered over two positions in ratio 0.533(4):0.466(4). Non-hydrogen atoms were anisotropically refined. The positions of hydrogen atoms (excluding atom H1) were calculated from known geometry and treated as riding, where the isotropic displacement parameters of these hydrogen atoms were fixed as a multiple of the equivalent isotropic thermal parameters of the parent atoms. For atom H1 the position was located on the Fourier difference map and refined with isotropic thermal parameters. Further experimental details and crystallographic data are presented in Table 1 and in the ESI.†

Hirshfeld surface analysis

The Hirshfeld surfaces¹⁰ were generated using Crystal Explorer 3.0¹⁶ based on results from X-ray studies. In Crystal Explorer, the internal consistency is important when comparing structures; therefore, bond lengths to hydrogen atoms were normalised to standard neutron values (C-H = 1.083 Å, O-H = 0.983 Å, N-H = 1.009 Å).¹⁷ The normalised contact distance (d_{norm}) based on both d_e (the distance from a point on the surface to the nearest atom outside the surface) and d_i (the distance from a point on the surface to the nearest atom inside the surface) and van der Waals radii of the atom, given by equation (1) enables identification of the regions of particular importance to intermolecular interactions.¹⁸ The value of the d_{norm} is negative (red colour) or positive (blue colour) when intermolecular contacts are shorter or longer than van der Waals separations, respectively.

$$d_{\text{norm}} = \frac{d_i - r_i^{\text{vdW}}}{r_i^{\text{vdW}}} + \frac{d_e - r_e^{\text{vdW}}}{r_e^{\text{vdW}}} \quad (\text{eq1})$$

Lipophilicity analysis

35 Lipophilicity is an indicator, which inform whether the molecule can easily pass through membranes or other barriers in our body or not. It is postulated that the more lipophilic the molecule is, the easier it goes through membranes due to stronger interactions with fatty acids of the lipid bilayer.¹⁹ The lipophilicity can be described as logP - the logarithm of the partition coefficient P. The coefficient P is defined as the ratio of the concentration of a substance in a non-polar phase to its concentration in the aqueous phase at thermodynamic equilibrium. The higher the polarity of the biologically active compound and the smaller the value of log P is, the less able the compound is to penetrate lipid membranes. In order to determine logP, the accepted standard solution is water as the polar phase and n-octanol as the non-polar phase. This system corresponds with the most polar and non-polar phase in a living organism. The value of log P has a significant impact on the fate of the drug in the body. In the literature, there are two methods for determining this parameter: experimental (direct and indirect) and theoretical ones.¹⁹ In this paper, we determined the lipophilicity for all compounds using the RP-TLC in the DMF/water solution.²⁰ A compound is lipophilic if its logP value is higher than 0. Results presented in Table 2 demonstrate that all compounds possess good lipophilicity.

Table 2 Lipophilicity index (logP) for all compounds

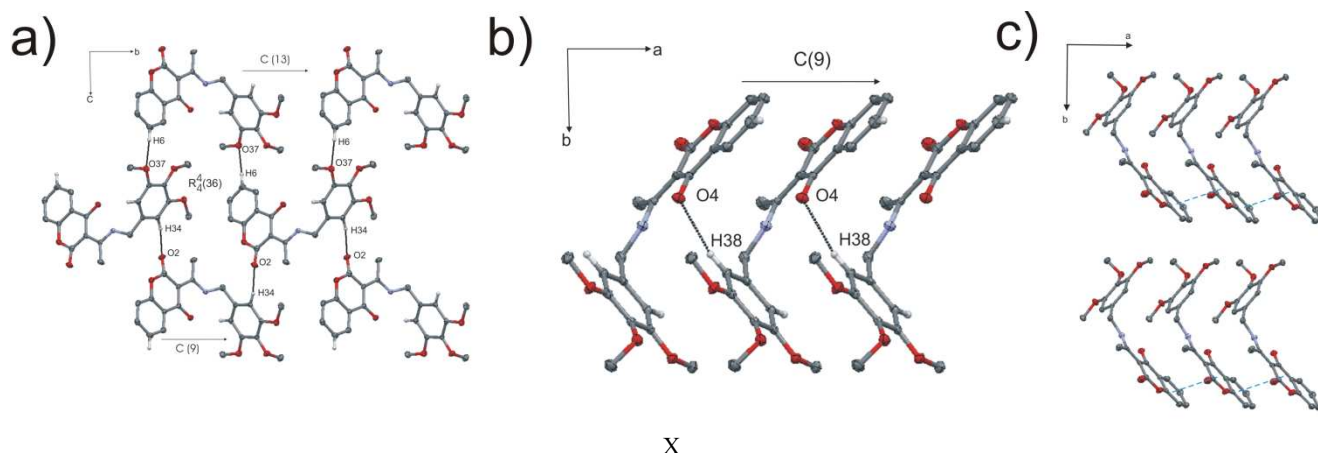
	log P
compound (I)	2.71 ± 0.63
compound (II)	4.07 ± 0.73
compound (III)	3.17 ± 0.74

The highest logP value was observed for compound (II) and decreased in compounds (III) and (I), respectively. However, as lipophilicity is a sum of many parameters more advanced research is needed to be sure whether tested compounds are able

Cite this: DOI: 10.1039/c0xx00000x

www.rsc.org/xxxxxx

ARTICLE TYPE



X

Fig. 3 a) Formation of 2D supramolecular network in (I) generated through C6-H6...O37ⁱ and C34-H34...O2ⁱⁱ hydrogen bonds b) Formation of the 2D sheet in 1 generated through C38-H38...O4ⁱⁱⁱ hydrogen bond c) Formation of two ribbons generated through π ... π stacking interactions between pyrane and benzene ring propagating along the [100] direction (compound I). H atoms are omitted for clarity

to pass through cell membranes. In order to obtain a theoretical value of log P, the program ALOGPs 2.1²¹ was used.

Results and discussion

Crystal structural description

The presented structures consist of a coumarin ring with (trimethoxy-benzylimino)-ethyl, (phenyl-trimethoxy-benzylimino)-methyl, and (imidazol-ethylimino)-methyl group substituted at position 3, for compounds (I), (II) and (III), respectively (Fig. 2). The coumarin backbone is planar and forms the following dihedral angles with substituents at atom C3: 85.7°, 83.2° and 57.7°, for (I), (II) and (III), respectively.

A common feature of the studied derivatives is an intramolecular hydrogen bond which forms an extra six-membered ring producing a graph set motif of S(6).²² The strength of intramolecular hydrogen bond is decreasing for (I), (II) and (III) with lengthening the N...O distances and decreasing angles <N-H...O. It seems that steric effect influences on the geometry of hydrogen bonds. On the other hand, the bond distances within the O=C-C=C-N-H conjugated bond ring systems (Table 3) indicate that these interactions can be classified as resonance-assisted hydrogen bonds (RAHB), proposed by Gilli.²³ The phenomenon of RAHBs may be described by the contribution of two tautomeric forms connected with the process of the proton transfer reaction: O/N-H...O \leftrightarrow O/N...H-O for homonuclear and heteronuclear systems. It was stated that for RAHBs a π -electron delocalization within the O=C-C=C-O/N-H keto-enol/amine chelate ring has been observed. The most characteristic feature for RAHBs of heteronuclear systems is: the equalisation of the lengths of the bonds C4-C3 (formally single) and C3=C31 (formally double) and shortening of the C31-N1 bond and lengthening of C4=O4 bonds with respect to other corresponding bonds that are not involved in the hydrogen

bond.²⁴ As can be observed in Table 3, the formally single bond C4-C3 appears shorter, the double C3=C31 bond appears longer, the C4=O4 bond is lengthened and C31-N1 is shortened with respect to reference values.²⁵ This suggests that the π -electron delocalisation effect is strongest for compound (I) and (II). Further geometrical parameters for intramolecular hydrogen bond distances, especially H1...O4 and N1...O4 (Table 4), confirmed this and are with agreement with original concept proposed by Gilli.²³

It is worth mentioning, that the concept of resonance-assisted hydrogen bonds is still under ongoing discussion,²⁶ however, in the case of other coumarin derivatives, the experimental charge density studies and application of source function²⁷ confirmed the existence of RAHBs for coumarin systems.²⁸

Table 3 Bond distances (Å) within hydrogen-bonding ring for the resonance assisted hydrogen bonds

	C4=O4	C4-C3	C3=C31	C31-N1
compound (I)	1.255(2)	1.435(2)	1.438(2)	1.313(2)
compound (II)	1.255(2)	1.436(2)	1.428(2)	1.319(2)
compound (III)	1.248(2)	1.446(2)	1.409(2)	1.310(2)

The solid-state structures of all compounds include a combination of N-H...N, C-H...O, C-H... π and π ... π stacking interactions. It is interesting to consider the substructures generated by each type of hydrogen bonds acting individually and the combination of all hydrogen bonds building the three-dimensional framework. The geometric parameters for hydrogen bonds in all structures are given in Table 4. In (I) the C6 and C34 atoms act as a donors in C-H...O hydrogen bonds with O37ⁱ [(i): -x, -1/2+y, 1-z] and O2ⁱⁱ [(ii): 1-x, 1/2+y, 2-z]. These two interactions form chains C(13)

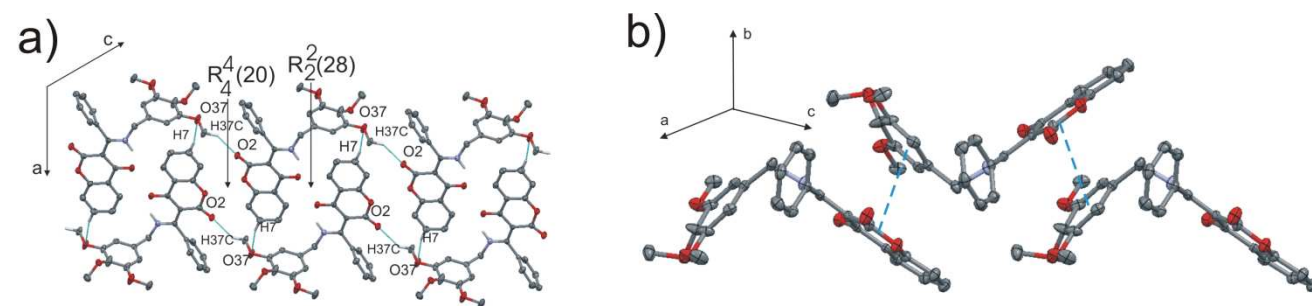
Cite this: DOI: 10.1039/c0xx00000x

www.rsc.org/xxxxxx

ARTICLE TYPE

Table 4 Geometrical parameters (in Å, °) for intra- and intermolecular hydrogen bonds; which in the Hirshfeld surface corresponds to H...O contacts and are marked as *la*, *la**(intramolecular hydrogen bond)

	d(D-H)	d(H...A)	d(D...A)	<D-H...A	symmetry
compound (I)					
N1-H1...O4	0.99(2)	1.66(2)	2.531(2)	143(2)	
C6-H6...O37 ⁱ	0.95	2.36	3.302(3)	170	-x, -1/2+y, 1-z
C34-H34...O2 ⁱⁱ	0.95	2.48	3.419(2)	170	1-x, 1/2+y, 2-z
C38-H38...O4 ⁱⁱⁱ	0.95	2.47	3.403(2)	168	-1+x, y, z
compound (II)					
N1-H1...O4	0.94(2)	1.74(2)	2.561(2)	144(1)	
C7-H7...O37 ^{iv}	0.95	2.46	3.375(2)	161	1-x, 1-y, -z
C371-H37C...O2 ^v	0.98	2.43	3.259(2)	142	1+x, y, 1+z
compound (III)					
N1-H1...O4	0.94(2)	2.11(2)	2.761(2)	125(2)	
N1-H1...N3 ^{vi}	0.94(2)	2.29(2)	3.047(2)	137(2)	1+x, y, z
C35-H35...O4 ^{vii}	0.95	2.53	3.152(2)	124	-1+x, y, z
C33-H33A...O1 ^{viii}	0.99	2.55	3.442(2)	149	-x, -y, -z
C36-H36...O2 ^{ix}	0.95	2.45	3.089(2)	124	-x, 1/2+y, 1/2-z

^a Footnote text.**Fig. 4** a) Formation of the 2D sheet in (II) generated through C7-H7...O37^{iv} and C371-H371...O2^v hydrogen bonds b) The π ... π stacking interaction between pyran and trimethoxybenzene rings in the crystal lattice of (II)

and C(9), respectively. Alternatively two chains are linked into the $R_4^4(36)$ ring extended to form an infinite two-dimensional layer on the plane (100) (Fig. 3a). Such layers are connected by C38-H38...O4ⁱⁱⁱ [(iii): -1+x, y, z] hydrogen bond forming chain C(9) along the [100] direction (Fig. 3b). This substructure is reinforced by π ... π interactions, which build 2-D ribbons extending along the [100] direction (Fig. 3c, Table 5). In the crystal lattice, one can observe significant C-H... π interactions for donors C351 and C371. The acceptor is a π -electron trimethoxybenzene ring in both cases (Fig. S1). It is worth mentioning, that the aromatic ring (C5-C10) is engaged in a lone pair... π interaction (C4=O4... π) in the crystal packing of

compound (I) (Fig. S1, Table S1). As demonstrated by Egli and co-workers C=O... π interactions play a crucial role in stabilising biomacromolecules.²⁹

In the case of crystal packing of (II), molecules are linked by a combination of C-H...O, C-H... π and π ... π stacking interactions. The formation of the molecular framework can be described as two different substructures. One substructure is formed by two C-H...O interactions. Hydrogen bonds: C7-H7...O37^{iv} and C371-H37C...O2^v; [(iv): 1-x, 1-y, -z, (v): 1+x, y, 1+z] generate one sheet of molecules with two rings, $R_2^2(28)$ and $R_4^4(20)$, respectively (Fig. 4a, Table 4). These sheets of molecules are linked by π ... π stacking interactions which is observed between pyran and

Cite this: DOI: 10.1039/c0xx00000x

www.rsc.org/xxxxxx

ARTICLE TYPE

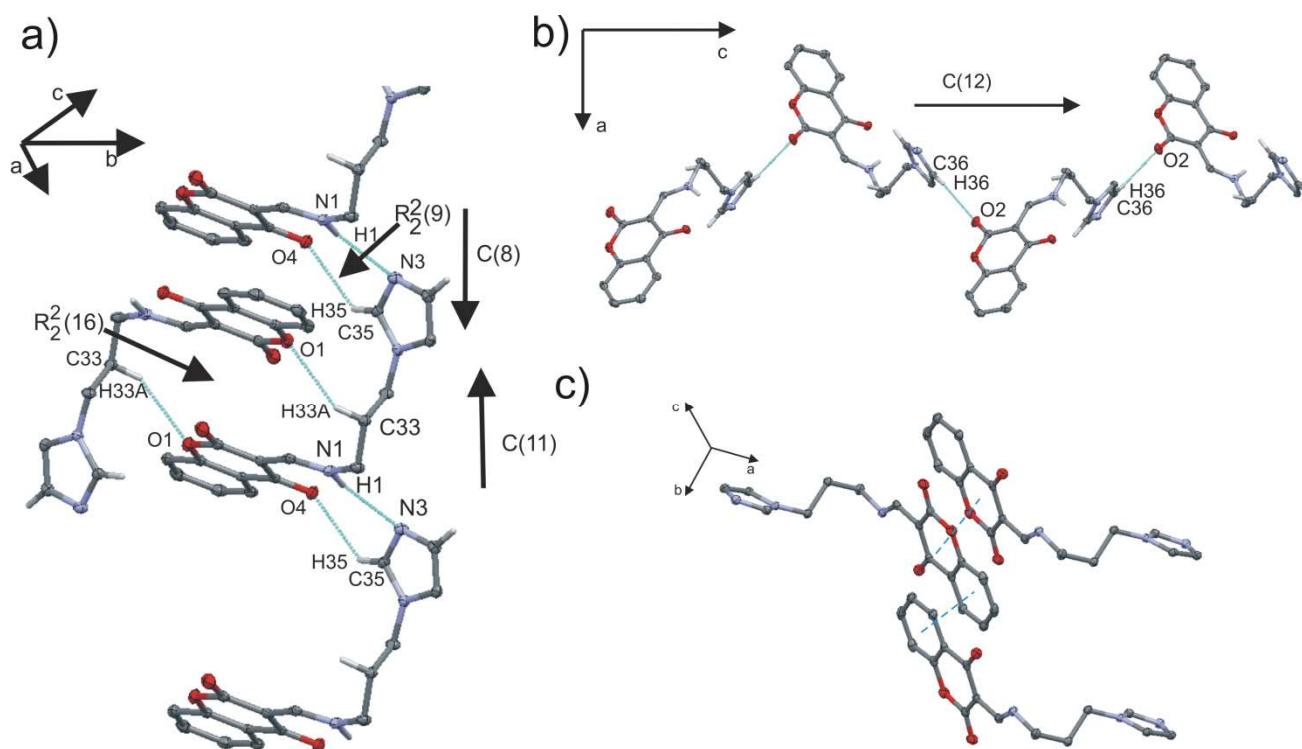


Fig. 5 a) Formation of the 2D sheet in (III) generated through N1-H1...N3^{vi}, C35-H35...O4^{vii} and C33-H33...O1^{viii} interactions b) Formation of the 1D chain in (III) generated through C36-H36...O2^{ix} hydrogen bonding c) The π...π stacking interactions between pyran and benzene rings in the crystal lattice of (III)

Table 5 Geometrical parameters (Å, °) for the π...π stacking interactions for all derivatives

	Cg(I)...Cg(J)	Cg(I)...Perp	Cg(J)...Perp	α	β	γ	symmetry
compound (I)							
Cg(1)...Cg(2)	3.8236(12)	3.4397(8)	3.4875(8)	1.73(9)	24.20	25.90	-1+x, y, z
compound (II)							
Cg(1)...Cg(3)	3.8567(9)	3.2075(7)	3.6383(7)	14.37(8)	19.38	33.73	x, 1/2-y, -1/2+z
compound (III)							
Cg(1)...Cg(1)	3.9930(16)	3.4704(5)	3.4703(5)	0	29.64	29.64	1-x, -y, -z
Cg(2)...Cg(2)	3.7846(16)	3.5130(5)	3.513(5)	0	21.84	21.84	-x, -y, -1-z

Cg(1), Cg(2), Cg(3) are centroids of pyran ring, benzene ring from coumarin moiety and trimethoxy-benzene ring, respectively; α - refers to the dihedral angle between planes (I) and (J), β - refers to angle between Cg(I)...Cg(J) vector and normal to the plane (I) and γ - refers to angle between Cg(I)...Cg(J) vector and normal to the plane (J)

trimethoxy-benzene rings (Fig. 4b, Table 5). In the crystal packing, further C313-H313... π and C371-H37C... π interactions, are also observed, where the π -electron rings are: benzene ring C5-C10 at $-x, -1/2+y, -1/2-z$ and the phenyl ring C311-C316 at $1+x,$

$y, 1+z$, respectively. C-H... π interactions aggregate two ribbons propagating along the [010] direction (Fig. S2, Table S1).

The crystal packing of (III) seems to be stabilised by a combination of intermolecular N-H...N, C-H...O, C-H... π

hydrogen bonds and $\pi \dots \pi$ stacking interactions. The N1 atom acts as a donor to N3^{vi} atom related by symmetry 1+x, y, z propagating the C(8) chain (Fig. 5a). The other chain C(11) is formed by the C35-H35... O4^{vii} interaction [(vii); -1+x, y, z]. However, both N1-H1...N^{vi} and C35-H35... O4^{vii} hydrogen bonds create the R₂²(9) ring (Fig. 5a). Moreover the C33 atom acts as a donor to oxygen atom O1^{viii} [(viii); -x, -y, -z] forming next dimeric ring R₂²(16) (Fig.4a, Table 4). In another substructure the C36 atom acts as a donor to the O2^{ix} atom in the molecule at -x, 1/2+y, 1/2-z, thus generating a 1D zig-zag chain along the [001] direction (Fig. 5b). The $\pi \dots \pi$ stacking interactions are seen in the crystal packing. They occur between parallel pyran rings, and parallel benzene rings (Fig. 5c, Table 5). The other substructure is formed by C7- H7... π interaction. Atom C7 is a donor to π electrons from the imidazole ring at -x, -1/2+y - 1/2-z. (see Fig. S3, Table S1). Moreover π -electrons from imidazole ring are acceptor for lone-pair... π interaction (Fig. S3, Table S1).

Hirshfeld surface

The Hirshfeld surface of titled compounds is illustrated in Fig 6 showing the surface that has been mapped over d_{norm} (-0.3 to 1.3 Å), shape index (-1.0 to 1.0 Å) and curviness (-4.0 to 0.4 Å). The surfaces are shown as transparent to allow the visualisation of a coumarin moiety in a similar orientation for all structures. The geometric parameters presented in Table 4 are summarised effectively in the deep red spots visible on the d_{norm} surfaces, indicative of hydrogen bonds and other weak interactions like H...H contacts. The unusually short normalised O...H distance can be seen in Hirshfeld surfaces as vivid red spots and are marked as *a*. The light red spots labelled *b* are due to H...C interactions. Other visible contacts marked as *c* correspond to H...N interactions in structure (III). The C-H...O interactions and intramolecular N-H...O hydrogen bond are represented as two spikes in the 2D fingerprint plots (Fig. 7) in the region 2.1 Å < ($d_{\text{e}}+d_{\text{i}}$) < 2.6 Å marked as *1a* and *1a**, respectively. However, the shortest $d_{\text{e}}+d_{\text{i}}$ = 2.1 Å is associated with C6-H6...O37ⁱ interactions. The proportion of O...H and H...O interactions contains 14.9% and 12.4% of the Hirshfeld surface for molecule (I). Other visible, yet light red spots in the Hirshfeld surface correspond to C-H... π interactions labelled *1b*. In the 2D fingerprint plot, this interaction is represented as mild spikes, where $d_{\text{i}}+d_{\text{e}}$ equals 2.74 Å. The proportion of C...H and H...C interactions is 9.4% and 7.7%, respectively. The dominant interaction in all compounds is H...H interaction, with the values equal 46%, 48%, and 40%, for compounds (I), (II) and (III), respectively. The $\pi \dots \pi$ interaction is also observed in compound (I) and is visible in the distribution of scattered points in the 2D graph – the region near 1.8 Å on the diagonal. Another characteristic feature of $\pi \dots \pi$ interactions is the pattern of red and blue triangles on the shape index. It is also visible on the curviness surface.

For compound (II), the 2D fingerprint plot has a different shape compared to the fingerprint plot of compound (I) without sharp spikes; however, the contribution of particular interaction does not differ significantly (Fig. 6 & 7). The bright red spot labelled *2a* is the C371-H37C...O2^v interaction with $d_{\text{i}}+d_{\text{e}}$ equalling 2.4 Å. Similar to structure (I), the proportion of O...H and H...O interactions is 12.8% and 10.8%. The light red spot

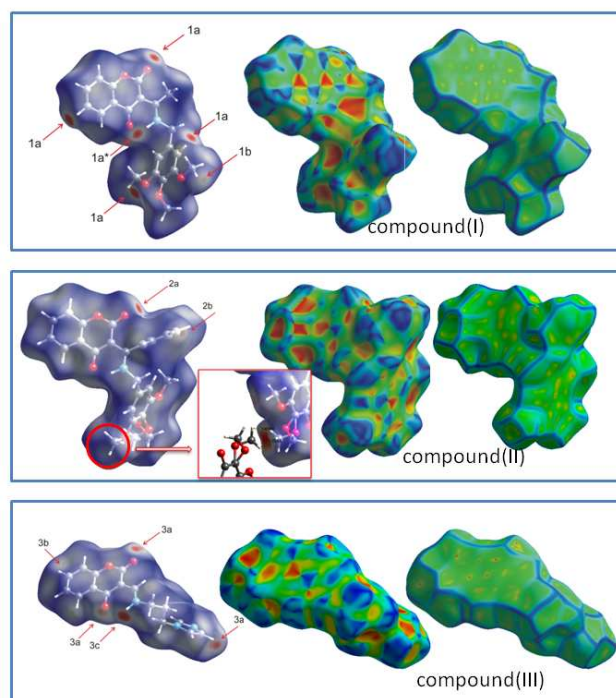


Fig. 6 Hirshfeld surfaces mapped with d_{norm} (left), shape index (middle) and curves for the presented compounds. For compound (II) the zoom of H...H interactions is presented

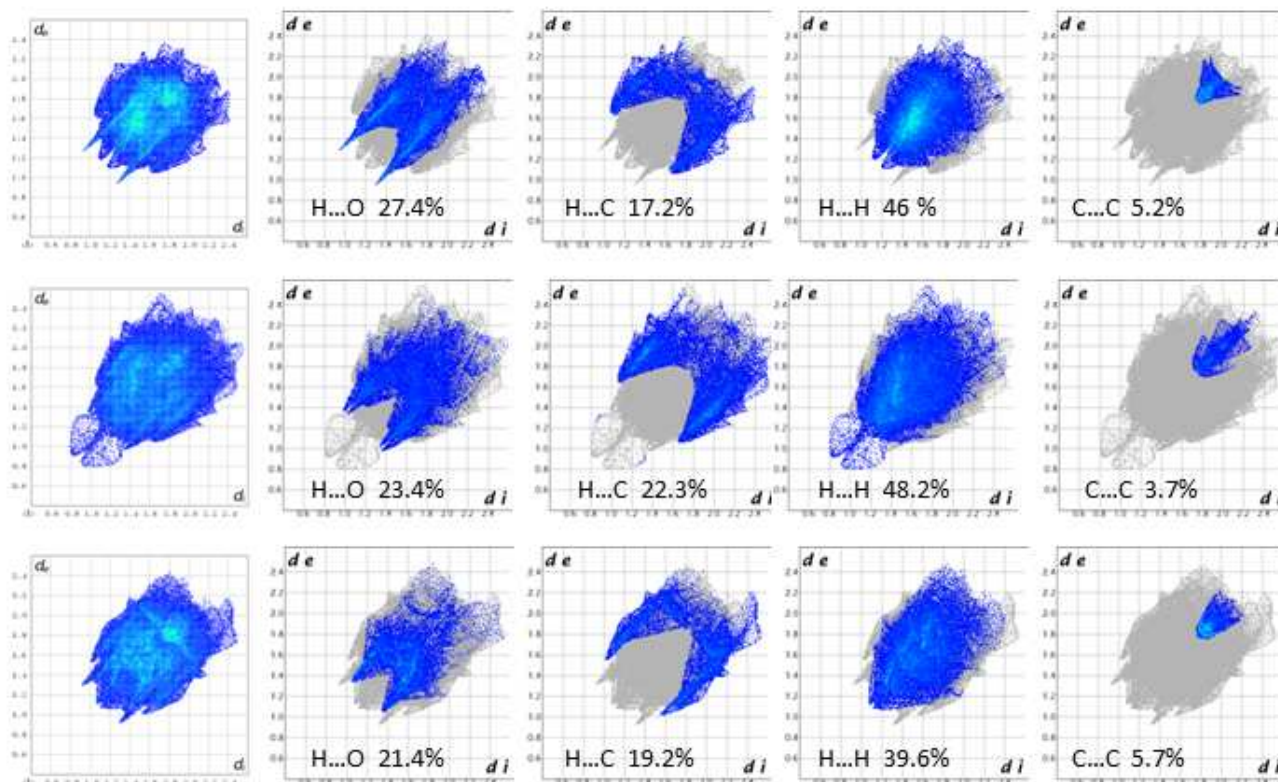
(*2b*) on the Hirshfeld surface appears to be due to C-H... π interactions with $d_{\text{i}}+d_{\text{e}}$ = 2.8 Å similar to compound (I). The proportion of H...C and C...H interactions varies from 9.7% to 12.8%. The C...C contact on the fingerprint plot is presented as characteristic stacking kite (see last column of Fig. 7), which is mainly attributed to $\pi \dots \pi$ interaction. On the shape index surface it is reflected by a pattern of red-blue triangles, but not so visible like for compound (I). The C...C contact includes only 3.7% of the Hirshfeld surface with equal d_{i} and d_{e} = 1.8 Å. The percentage of H...H contact is 48% - the maximum among other coumarin derivatives. Additionally, the completely different distribution of scattered points on the fingerprint plot is observed with very short distance d_{i} and d_{e} = 0.8 Å. The shortest H...H distance is visible as the vivid red spot and could be attributed to the contact between disordered hydrogen atoms from methyl group. (Fig. 6). The lowest C...C contact and the highest H...H contact seems to be related to more bulky spatial structure of molecule (II) in itself.

On the Hirshfeld surface of structure (III) we can distinguish three types of interactions: *3a* is associated with H...O contact, *3b* represents H...C contact, while H...N interaction is labelled *3c* (Fig. 6). The intramolecular N-H...O interaction and C-H...O intermolecular interactions are reflected in the 2D fingerprint plot in the region 2.45 Å < ($d_{\text{i}}+d_{\text{e}}$) < 2.75 Å. The C-H... π interaction is presented by spikes where $d_{\text{i}}+d_{\text{e}}$ equals 2.8 Å similar to compound (I) and (II). The other interaction, presented by large bright red spot on the Hirshfeld surface and the longest spikes on the fingerprint plot, is connected with N1-H1...N3^{vi} intermolecular hydrogen bond. Sum of $d_{\text{i}}+d_{\text{e}}$ amounts 2.25 Å. This kind of hydrogen bond is only observed for structure (III). The C...C contact contribution in the Hirshfeld surface is larger than for compound (I) and (II), however d_{i} and d_{e} equals 1.8 Å,

Cite this: DOI: 10.1039/c0xx00000x

www.rsc.org/xxxxxx

ARTICLE TYPE



X

Fig. 7 Fingerprint plots of compound (I) – top row, compound (II) – middle row and compound (III) – bottom row: full (left) and resolved into H...O, H...C, H...H, C...C contacts showing the percentages of contacts contributed to the total Hirshfeld surface area of molecules

5 the same as for compound (I).

Contribution of different interactions to Hirshfeld surface for related structures from CSD

The relative contribution of the different interactions to the Hirshfeld surface was calculated for presented compounds as well as for other similar coumarin derivatives available in the Cambridge Structural Database (version 1.15 CSD 2013 release)³⁰ including coumarin derivatives determined by us.**Error! Bookmark not defined.**³¹ A number of structures found is 15 with different substituents on the coumarin moiety
15 (scheme of query used in database search contains coumarin backbone with double bond at atom C3, see Scheme S2).

The dominant interaction in coumarin derivatives is H...H interaction (Fig. 8). The contribution to the Hirshfeld surface is in the range 28% to 50.8% for UPATAH³² and PUMJIR³³. The
20 smallest H...H contribution to the Hirshfeld surface for UPATAH³² corresponds with evenly distributed other interactions for that structure. The investigation of the crystal packing of UPATAH³² displays a characteristic type of layered structure, where molecules lie on planes separated by 3.45 Å

25 (Fig. S4). The same tendency is observed for other available Hirshfeld surface analysis of coumarin derivatives.³⁴

The π ... π stacking interaction is reflected in the C...C interactions for which a contribution to the Hirshfeld surface vary from 0% to 7.9% for all structures. Among eighteen analysed
30 structures four of them has significantly small contribution 0% to 0.8% since the hetero ring (tetrahydropyran) is not planar for those structures (PUMJIR,³³ LAPVAB,³⁵ RUZXEP,³⁶ RUZXAL³⁶). However, for the remaining structures the C...C contribution is in the range 1.4% to 7.9% which corresponds with
35 the pattern of red and blue triangles on the shape index surface (Fig. 6). The next significant percentage of the contribution to the Hirshfeld surface is for O/N...H contact (green and red colour on Fig. 8) and varies from 17.4% to 37.6%. The contributions of C...H interactions vary from 10.1% to 30.5% in WACWAA³⁷
40 and LAPVAB³⁵, respectively. Since the contributions of C...H interactions are related to the lipophilicity index, the more detailed analysis of C...H contribution is presented below.

Lipophilicity index vs C...H contact

It was found that the contribution of C...H interactions to the

Cite this: DOI: 10.1039/c0xx00000x

www.rsc.org/xxxxxx

ARTICLE TYPE

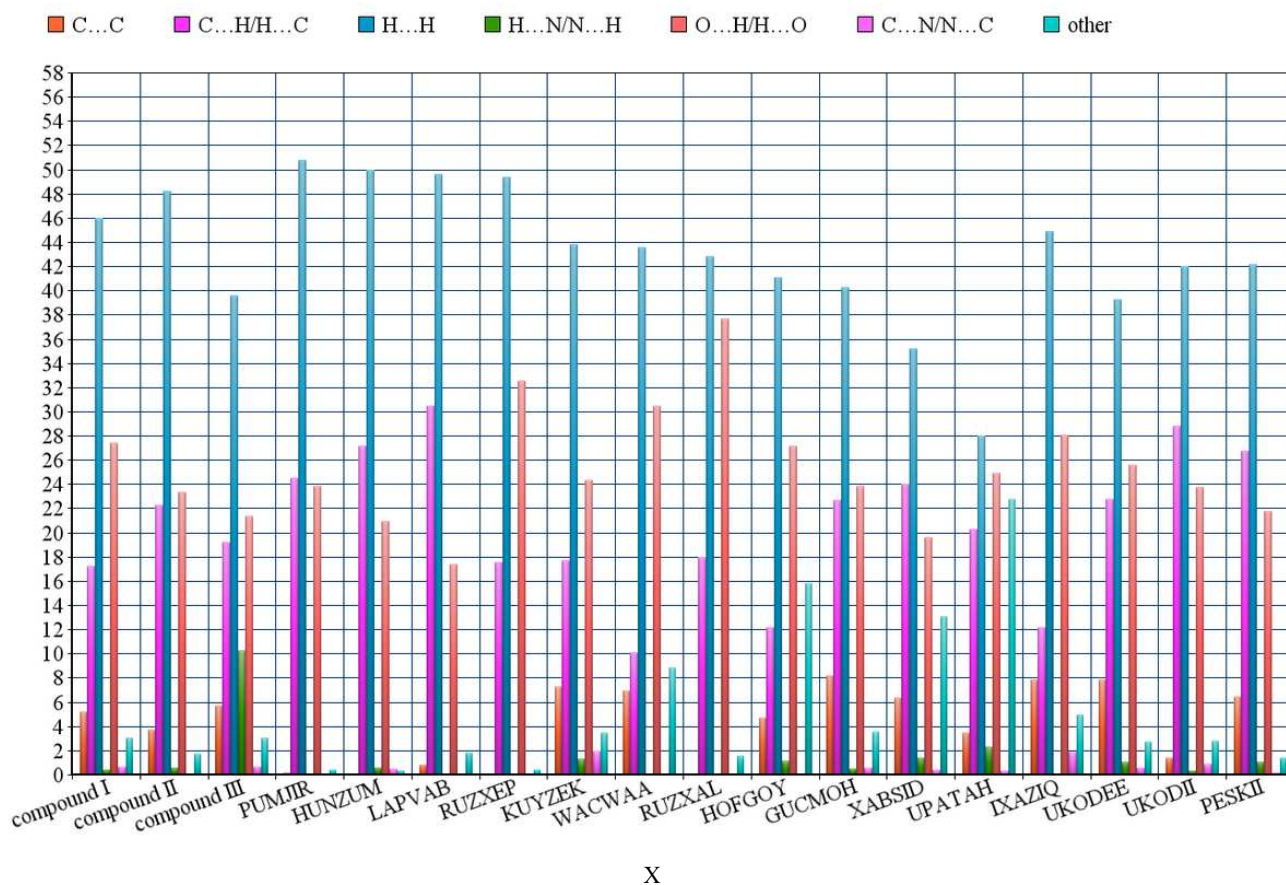


Fig. 8 Relative contributions of various intermolecular contacts to the Hirshfeld surface area in compound (I), (II) and (III) and other related structures retrieved from the CSD

5 Hirshfeld surface corresponds with logP value. LogP describes lipophilicity which refers to an ability of molecule to dissolve in non-polar solvents. We compare the logP value with the contribution of C...H interactions to the Hirshfeld surface for four coumarin derivatives; three presented here and one IXAZIQ³¹ for which we determined logP earlier.^{8a} Among the four structures the highest logP value was reported for compound (II) (4.07%), relating to the highest C...H (22.3%) contribution in the Hirshfeld surface. The lowest logP value and lowest C...H contribution is observed for compound IXAZIQ (-0.34% and 12.2%, respectively). For the four structures, we found a tendency when logP is decreasing with the percentage of C...H contribution to the Hirshfeld surface.

Conclusion

20 Three new coumarin derivatives have been synthesised and determined by X-ray crystallography. Our study has focused on analysis of the crystal structures, interactions and different

structural motifs.

25 The structural feature of these compounds is the appearance of two types of motifs: R (rings) and C(chains) formed by weak C-H...O hydrogen bonds. In every structure these interactions lead to building the 2D supramolecular network of bonds. In case of crystal structure (II) and (III) the successive 2D sheets of molecules are linked by π ... π interactions, while these are additionally enhanced by C-H...O interactions in crystal structure of (I).

30 Since, the presented compounds exhibit biological activity, we elucidate the lipophilicity parameter (logP) and compare it with respect to different intermolecular interactions. It was seen that 35 the contribution of C...H interactions to the Hirshfeld surface correlates well with logP value.

Acknowledgements

40 The high-resolution measurement of compound (III) was carried out within the projects I-20090042EC and I-20110099EC at the light source DORIS III at HASYLAB/DESY, Hamburg,

Germany. The research leading to these results has received funding from the European Community's Seventh Framework Programme (FP7/2007-2013) under grant agreement No. 226716. Financial support from the Medical University of Lodz (grant No 5 503/3-066-02/503-01 to E. B. Dr. Lilianna Chęcińska, Dr. Piotr Seliger is gratefully acknowledged for stimulating discussion and technical support. Prof. Joachim Kusz from the University of Silesia is gratefully acknowledged for the X-ray measurements of compound (I) and (II). Miss Małgorzata Telesiewicz is gratefully
10 acknowledged for technical support.

Notes and references

^a *Structural Chemistry and Crystallography Group, University of Lodz, Pomorska 163/165, 90-236 Łódź, Poland. Tel: +48 42 635 57 41; E-mail: malecka@uni.lodz.pl*

^b *Department of Cosmetic Raw Materials Chemistry, Medical University of Lodz, Muszyński 1, 90-151 Łódź, Poland. E-mail: elzbieta.budzisz@umed.lodz.pl*

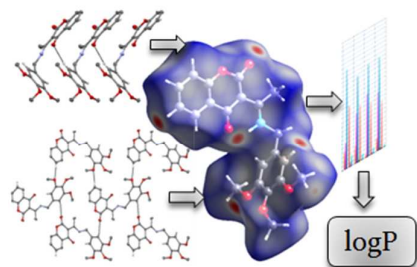
† Electronic Supplementary Information (ESI) available: It contains
20 Scheme S1 (query scheme in the database, Fig. S1-S4, crystallographic data in cif format, for CCDC 990515-990517- See DOI: 10.1039/b000000x/

- 1 (a) G. R. Desiraju, *Science* 1997, **278**, 404.(b) Top. Curr. Chem. *Design of Organic Solids*; Weber, E.,Ed.; Springer-Verlag: Berlin, 1998; **198**.
- 2 G.R. Desiraju, *Angew. Chem., Int. Ed. Engl.* 1995, **34**, 2311. (b) A. Nangia, G. R. Desiraju, *Top. Curr. Chem.* 1998, **198**, 57.
- 3 T. Usui, *Endocrine J.* 2006, **53**,7.
- 4 I. Malonov, I. Kostova, T. Netzeva, S. Konstantinov, M. Karaivanova, *Arch. Pharm. Pharm. Med. Chem.*, 2000, **333**, 93.
- 5 (a) T. Patonay, G. Litkei, R. Bogнар, J. Erdei, G. Miszti, *Pharmazie* 1984, **39**, 84. (b) U.S. Weber, B. Steffen, C. Sigers, *Res. Commun. Mol. Phatol. Pharmacol.*, 1998, **99**, 193.
- 6 (a) D. Egan, R. O'Kennedy, E. Moran, D. Cox, E. Prosser, R.D. Thornes, *Drug Metab. Rev.* 1990, **22**, 503. (b) M. A. Musa, J. S. Cooperwood, M.Omar, F. Khan, *Curr. Med. Chem.*, 2008, **15**, 2664. (c) F. Borges, F. Roleira, N. Milhazes, L. Santana, E. Uriarte, *Curr. Med. Chem.*, 2005, **12**, 887.
- 7 M. Recanatini, A. Cavalli, *Bioorg. Med. Chem.* 2004, **5**, 207.
- 8 (a) E. Budzisz, E. Brzezińska, U. Krajewska, M. Różalski, Eur. J. Med. Chem. 2003, **38**, 597. (b) K. V. Sashidara, S. Avula, K. Sharna, G. R. Palanti, S. R. Bathula, *Eur. J. Med. Chem.* 2013, **60**, 120-127. (c) S. Y. Park, M. Ebihara, Y. Kubota, K. Fuabiki, M. Matsui, *Dyes & Pigments*, 2009, **82**, 258-267.
- 9 (a) G. R. Desiraju, *Acc. Chem. Res.*, 2002, **35**, 565. (b) G. A. Jeffrey, *An Introduction to Hydrogen Bonding*; Oxford University Press: Oxford, U.K., 1997. (c) G. R. Desiraju, T. Steiner, *The Weak Hydrogen Bond in Structural Chemistry and Biology*; Oxford University Press: Oxford, U.K., 1999. (d) G. R. Desiraju, *Nature*, 2001, **412**, 397. (e) T. Steiner, *Angew. Chem., Int. Ed.* 2002, **41**, 48.
- 10 (a) M. A. Spackman, P. G. Byrom, *Chem. Phys. Lett.* 1997, **267**, 215. (b) M. A. Spackman, D. Jayatilaka, *CrystEngComm*, 2009, **11**, 19. (c) M. A. Spackman, J. J. McKinnon, *CrystEngComm*, 2002, **4**, 378. (d) J. J. McKinnon, D. Jayatilaka, M. A. Spackman, *Chem. Commun.*, 2007, 3814. (e) M. A. Spackman, J. J. McKinnon, D. Jayatilaka, *CrystEngComm*, 2008, **10**, 377. (g) F. L. Hirshfeld, *Theor. Chim. Acta*, 1977, **44**, 129. (h) H. F. Clausen, M. S. Chevallier, M. A. Spackman, B. B. Iversen, *New J. Chem.*, 2010, **34**, 193.
- 11 B. A. Domin, W. B. Mahony, T. P. Zimmerman; *Biochem Pharmacol.*; 1991, **42**, 147.
- 12 CrysAlis RED Oxford Diffraction, 2008, Oxford Diffraction Ltd, Yarnton, England.
- 13 W. Kabsch, *J. Appl. Cryst.*, 1993, **26**, 795.
- 14 S. K. J. Johnas, W. Morgenroth, E. Weckert, *Annual Report, HASYLAB/DESY*, 2006, 325.
- 15 G. M. Sheldrick, *Acta Cryst.*, 2008, **A64**, 112.
- 16 (a) M. A. Spackman, J. J. McKinnon, *CrystEngComm*, 2002, **4**, 378. (b) M. A. Spackman, D. Jayatilaka, *CrystEngComm*, 2009, **11**, 19. (c) M. A. Spackman, J. J. McKinnon, D. Jayatilaka, *CrystEngComm*, 2008, **10**, 377.
- 17 F. H. Allen, D. G. Watson, L. Brammer, A. G. Orpen, R. Taylor, *International Tables for X-ray Crystallography*, 2006, **Vol. C**, ch. 9.5, 790–811. Amsterdam: Kluwer Academic Publishers.
- 18 J. J. McKinnon, M. A. Spackman, A.S. Mitchell, *Acta Cryst.*, 2004, **B60**, 627.
- 19 A. Pyka, M. Babuska, M. Zachariasz, *Acta Poloniae Pharm.-Drug Research*, 2006, **63**, 159.
- 20 K. Mazak, J. Vamos, A. Nemes, A. Racz, B. Noszal, *J. Chrom. A*, 2003, **996**, 195-203.
- 21 <http://www.vcclab.org/lab/alogps/>
- 22 (a) M. C. Etter, *Acc. Chem. Res.*, 1990, **23**, 120. (b) J. Bernstein, R. E. Davis, L. Shimoni, N-L. Chang, *Angew. Chem. Int. Ed. Engl.* 1995, **34**, 1555.
- 23 (a) P. Gilli, F. Bellucci, V. Ferretti, V. G. Bertolasi, *J. Am. Chem. Soc.*, 1989, **111**, 1023. (b) G. Gilli, P. Gilli, *J. Mol. Struct.*, 2000, **552**, 1.
- 24 V. Bertolasi, P. Gilli, V. Ferretti, G. Gilli, *Acta Cryst.*, 1994, **B50**, 617.
- 25 F. H. Allen, D. G. Watson, L. Brammer, A. G. Orpen, R. Taylor, 2006, *International Tables for X-ray Crystallography*, Vol. C, ch. 9.5, pp. 790–811. Amsterdam: Kluwer Academic Publishers.
- 26 I. Alkorta, J. Elguero, O. Mo, M. Yanez, J. E. del Bene, *Mol. Phys.* 2004, **102**, 2563. (b) I. Alkorta, J. Elguero, O. Mo, M. Yanez, J. E. del Bene, *Chem. Phys. Lett.*, 2005, **411**, 411.
- 27 C. Gatti, F. Cargnoni, L. Bertini, *J. Comput. Chem.*, 2003, **24**, 422.
- 28 (a) M. Malecka, L. Chęcińska, A. Rybarczyk-Pirek, W. Morgenroth, C. Paulmann, *Acta Cryst.*, 2010, **B66**, 687. (b) M. Malecka, L. Chęcińska, C. Paulmann, *Struct. Chem.*, 2012, **23**, 801.
- 29 M. Egli, S. Sarkhel, *Acc. Chem. Res.*, 2007, **40**, 197.
- 30 Cambridge Crystallographic Data Centre 2011. ConQuest, Version 1.13. CCDC, 12 Union Road, Cambridge, UK; http://www.ccdc.cam.ac.uk/products/csd_system/.
- 31 M. Malecka, S. J. Grabowski, E. Budzisz, *Chem. Phys.*, 2004, **297**, 235.
- 32 M. Helliwell, D. A. Nasiopoulou, P. A. Harris, A. Kotali, J. A. Joule, *Acta Cryst.*, 2011, **E67**, o1014.
- 33 X. Han, X. Lu, *Org.Lett.*, 2010, **12**,108.
- 34 S. K. Seth, D. Sarkar, A. D. Jana, T. Kar, *Cryst. Growth Des.* 2011, **11**, 4837.
- 35 M. Asad, C.-W. Oo, H. Osman, J. H. Goh, H.-K. Fun, *Acta Cryst.*, 2010, **E66**, o3129.
- 36 F. H. Osman, N. M. A. El-Rahman, F. A. El-Samahy, I. S. A. Farag *Phosphorus,Sulfur,Silicon,Relat.Elem.*, 2003, **178**, 531.
- 37 S. Vijayakumar, S. Murugavel, D. Kannan, M. Bakthadoss, *Acta Cryst.*, 2012, **E68**, o791.

Structural framework of biologically active coumarin derivatives. Crystal structures and Hirshfeld surface analysis

Magdalena Małecka,* Elzbieta Budzisz

Table of Contents entry



The relation between lipophilicity parameter ($\log P$) and the contribution of C-H... π interactions to the Hirshfeld surface has been investigated.